LA-UR -85-3625

CONF-850770--13

Los Alamos National Laboratory is operated by the University of California for the United States Department of Energy under contract W-7405-ENG-36

TITLE CONTROLLED POWDER MORPHOLOGY EXPERIMENTS IN MEGABAR 304 STAINLESS STEEL COMPACTION

AUTHOR(S) Karl P. Staudhammer, MST-7
Kaye A. Johnson, MST-13

LA-UR--85-3625

DE86 002416

SUBMITTED TO International Conference on Metallurgical Applications of Shock-Wave and High-Strain-Rate Phenomena, Marcel Dekker Pub. Portland, OR - July 28 - August 1, 1985

Los Alamos National Laboratory
Los Alamos, New Mexico 87545

FORM NO 836 R4

CONTROLLED POWDER MORPHOLOGY EXPERIMENTS IN MEGABAR 304L STAINLESS STEEL COMPACTION

K. P. STAUDHAMMER and K. A. JOHNSON

Materials Science and Technology Division
Los Alamos National Laboratory
Los Alamos, New Mexico USA 87545

Experiments with controlled morphology including shape, size, and size distribution were made on 304L stainless steel powders. These experiments involved not only the powder variables but pressure variables of 0.08 to 1.0 Mbar. Also included are measured container strain on the material ranging from 1.5% to 26%. Using a new strain controllable design it was possible to separate and control, independently, strain and pressure. Results indicate that powder morphology, size distribution, packing density are among the pertinent parameters in predicting compaction of these powders.

I. INTRODUCTION

Shock consolidation of powders is currently being investigated by many experimenters for several important reasons. The first is the potential for inexpensive fabrication, compaction, or assembly offered by explosives. The second is the very short reaction time of explosive systems. Many modern engineered materials of potential are of such morphologies,

mixtures, or meta-stable phases that the extremely short reaction time of explosives creates an opportunity to assemble such unique fibers and powders without the loss of their inherent special characteristics. In addition there are those standard materials for which explosives also offers more energetic and cost effective method of assembly, such as ceramics.

A broad spectrum of papers have been written on explosive consolidation, studying material types, shock system designs, and properties and/or results of the studies. More recently, a greater portion of papers have been published that recognize the need to better characterize the starting powder. This sort of characterization is as necessary for the understanding of powder response in shock compaction as it is with "normal" powder technology. (With the very high strain rate of shock compaction, it may be even more important) Apparently, it has been much easier to adjust the external shock parameters, attempting to create a "window" of favorable shock conditions to fit a particular powder [1,2]. However, not all studies have had even mediocre success because the window can vary as the powder density, morphology and other characteristics changes. In addition, many studies are plagued with a wide variety of non-consolidated materials and cracks, usually ascribed to the inherent design, nature of the shock wave and explosive variability. However, limited attention has been paid to the relationship between powder characteristics and the shock compacted properties.

This study shows that the characteristics of the powder itself are a significant feature in attempting to predict the nature of the compact in a given system. For example, a nominal difference in preshock packing density, can have a strong effect on the nature of the consolidation.

Using a well characterized shock system [3] and with a substantial data base on solid 304L SS (and other metals) [4], selected 304L SS powders with spherical morphology were used in this study. Parameters of importance to the study were strain, strain rate, size and size distribution, and morphology. In addition such combinative relationships such as local strain, residual temperature ΔT_R, contact points and initial packing density are significant.

This study was designed to explore extreme conditions for compaction and consolidation and is not suggested for part fabrication. It is a unique method for pressure, strain and temperature variations in one shot, one sample.

II. MODEL

The dynamic consolidation of powders involves several distinct processes. For the material considerations, the initial packing which consequently affects density and subsequently affects the strain temperature conditions can be characterized.

The packing density of a powder is a function of size, size distribution and morphology. To simplify the model and interpretation, spherical powders were selected. The closest packing of monosized spherical powders can easily be defined and is 74% of the theoretical density. The actual density of random packed spheres is worked out in theory [5-8] and also has been demonstrated with real spheres in an excellent paper which also includes wall effects [9]. For example, a simplified model of a 2 dimensional system would be the filling of the interstices of a closed packed system. In this geometry the ratio of the interstices diameter (d) to that of the larger circle diameter (D) is d/D = 0.125, consequently, the area packing density is thus increased to 92.6% from 89.8%.

In 3 dimensional systems assuming FCC (or HCP) packing the interstitial sites are larger. Application and investigation of these points has been developed by [9]. By using these concepts, variations in density can be achieved by manipulating the size, size mixture and size fraction of ternary packing to achieve the desired packing density. Provided that the ratio of the sample holder diameter to that of the powder diameter is greater than 10, edge effects can be ignored. For our 0.65 cm ID tube the worst ratio is 42.5 (100 mesh powder). Finer powder have equivalent packing efficiency ratios. The packing density relations as given by [9] are as follows:

$$\% \text{ Theoretical density} = 100 \quad 1 - \frac{\upsilon_n \; X_n}{\upsilon_n X_n + V}$$

n = number of components in packing

υ_n = volume fraction of voids in finest component

X_n = volume fraction of finest component

V = a constant; volume of solid material

The densest packing of binary sizes occur at 72.7% coarse powder (7 mesh) mixed with 27.3% medium powder (100 mesh), achieving an 84% theoretical density. The densest ternary packing that can be expected is 93.5%. Thus, by applying equation 1 the packing density can be varied between 74% for monosized spheres to 93.5% for appropriate ternary mixture packing. Even for perfect spheres these values are only limiting values due to packing defects such as point, line and planar faults as well as edge effects. The statistical theory and approach for handling random packing has been well covered by [5,8].

Another point that needs clarification is contact points; ie particle to particle contact. If the powder size is changed from a given monosize to a smaller monosize, the density will remain the same, however, the number of contact points increase per unit volume. Similarly, as one changes the binary and tertiary packing density, the number of contact points greatly increases. An increase in the number of contact points (ie, an increase in density of the packed powder) reduces the maximum local strain and strain distribution. As the strain is reduced, concomitantly the residual temperature is reduced.

III. EXPERIMENTAL

A. STARTING MATERIAL

Powders of 304L stainless steel was chosen for this investigation because of its availability, size and morphologies. Also, in addition to the available data base for both powder and solid 304L shock response [3,4].

The material used in this study was obtained from Valimet Inc. The chemical analysis of this powder was (wt%), 18.5 Cr, 10.5 Ni, 0.15 Co, 0.028 C, and the balance Fe and was produced by a spin atomization process. While 304 SS powder may be as irregular as shown in Fig. 1, the powders used in this study are much more spherical as shown in Fig. 2. To achieve our goal of studying such parameters as contact points, initial packing density, the as-received powder was size sorted to make available several monosized fractions. The powders reported here are nominally 150 μm for the 100 mesh, 88 μm for the 170 mesh, and 45 μm for the 325 mesh

B. SHOCK COMPACTION METHOD

The experimental design and explosive system is the same as that used and described in another paper in this volume by the authors [3]. Shock pressure in the powder samples was calculated using the correct equation of state but with a homogeneous appropriate reduced density. The code used does not allow the powder to shock up to full density so the profiles are minimums. Figure 3 shows the calculated pressures near the OD of a 57% theoretical density 304L SS powder. The pressure increases towards the central axis as well as from top to bottom as shown. The radial and length distributions are given in more detail in another paper for solid 304L SS in this volume by the authors [3].

The shock tube assembly containing the powders of interest was made from 304L SS as it minimized the hydrocode calculations as well as improved weldability. The shock tubes were evacuated to less than 0.13 Pa prior to welding.

C. DENSITY MEASUREMENTS

Initial packing densities were obtained by dividing the full loaded powder weight by the calculated volume of the shock tube. Densities were varied by changing the size and size distribution of the starting powder.

D. CHARACTERIZATION

Samples were examined by a variety of techniques. The primary method of analysis was Scanning Electron Microscopy (SEM) supported by optical microscopy. Energy Dispersive X-ray analysis (EDX) was used to confirm chemical analysis. Preshock particle size analysis was performed on SEM images using a Dapple system with Los Alamos modified software. The post shocked samples were cut perpendicular to the central axis at selected distances correlating to specific pressures and local strains. A slow speed diamond saw was used for sectioning. The metallographic samples were chemically etched by standard techniques and argon ion etching prior to analysis.

IV. RESULTS

Figure 4 is a schematic of a typical longitudinal cross section of a post shot powder holder. The pressure increases from top to bottom along the central axis and at any point (from the top) decreases with increasing radius. The local strain increases with axial length (from the top) and is a function of the momentum trap height and design [3]. However, the local strain for these powder samples is far more complex than for a solid sample. The powder particle strain magnitude can exceed strains of 100%. Consequently, the temperature rise is greater for equivalent shock designs than for a solid sample. A diameter shrinkage of approximately 13% is obtained for the powder compacts having initial packing densities between 47 to 77 percent and remains fairly constant from the top to the bottom of the powder holder. The central axis, in all of the shots reported here contained a mach stem and associated molten region. The size of the mach stem hole is irregular due to solidification, therefore, the parameter that should be focused on is the melt zone radius adjacent to it. The molten region will vary with distance from the top (i.e. increasing pressure) and the initial powder density of the 304L SS. Surrounding the molten region is the compacted/consolidated powder. It contains regions that are under and over compacted, as well as appropriately consolidated. The impingement of the mach stem jet on the end plug causes a reaction and/or alloying with the capsule end plug.

A. 100 MESH 304L STAINLESS STEEL POWDER

Figure 5 is an optical micrograph of a cross-section view of a sample section perpendicular to the shock direction having an initial packing density of 47%. This section was taken 3.8 cm from the top and experienced a pressure of approximately 0.66 Mbar in the center to approximately 0.07 Mbar on the outer diameter, this pressure profile is illustrated in Fig. 3. Shown in Fig. 5a is the solidification shrinkage due to the excessive heat generation resulting from a high pressure and strain heat contribution. At a larger radius is the retained molten material with the extremely fine dendrite morphology shown in Fig. 5b

The dendrite structure is similar to that of rapidly solidified dendrites having cooling rates between 10^3-10^4/sec. At a larger radius is a zone of consolidated powder with some local interparticle melting. Shown in Fig. 5c is the transition region between the melted and consolidated portions. Note that the mach stem melt solid interface (marked by arrow) does not protrude into the prior powder particle interfaces but rather cuts thru the particles themselves in a smooth cylindrical plane. Clearly different in cause and nature from the interparticle melting in the consolidated outer portions.

3. 170/325 MESH 304L STAINLESS STEEL POWDER

A binary powder blend of 12 vol% - 170 mesh and 78 vol% - 325 mesh resulted an initial packing density of 57%. A higher initial density should decrease the particle strain and subsequent temperature rise. To elucidate the powder particle deformation, the powder blend was gold plated Approximately 20 nm of gold was plated on top of a electroless nickel strike. A cross-section of a shock consolidated 57% theoretically dense 304L SS powder is shown in the optical micrograph of Fig. 6. This sample was taken further down from the top of the tube and experienced a higher pressure (1.0 Mbar to approximately 0.4 Mbar) than the 47% dense powder (100 mesh) (pressure approximately 0.66 to 0.07 Mbar) shown in Fig. 5.

The radial cracks observed here are due to the solidification shrinkage of the molten region. The consolidated regions are clearly less than 1 Mbar pressure and it appears that approximately 0.4 Mbar is more than sufficient pressure for the 57% dense powder to consolidate. The pressure to melt as based on the hydro code calculations is 0.69 Mbar. This radial distance is indicated by the arrow in Fig. 6. This transition zone in Fig. 6 are shown in Fig. 7a-b.

Figure 7a shows the consolidated region next to the melt region. This is the region of highest pressure and strain that this packing density can undergo without melting. The calculated shock wave direction is indicated in Fig. 7a relative to the shock wave. Note the deformation geometry and strain magnitude of the powder particles. They are cup shaped on the back side of the shock direction with the shock

deformations have the deformation parallel with the shock wave direction. This is indicative of particle acceleration. These features are typified in Fig. 7b at points marked A and b. The regions marked C are gold/stainless alloying. The particle marked D is partially melted and typical of particles in the immediate adjacent melt zone. The stem melt region has a smooth straight interface relative to the powder particle surface. Evident from particles in this interface is that only limited melting occurred between particles inspite of the enormous heat (ie melting) in the melt region.

At lower pressure and lower local strain, the particle deformation and particle strain magnitude are quite different. The strain magnitude in most particles is much less and the deformation is limited to the spherical powder occupying a polyhedral shape having an average maximum/minimum diameter ratio close to 1. This is depicted in Fig. 8 which experienced a peak pressure of 0.07 Mbars and is under compacted. The scanning electron micrograph shown in Fig. 9 illustrates the polyhedra geometry typical of the low pressure region. Note that the fracture is interparticle. The outer region (OD of the powder compact) of the holder as shown in Fig. 9a did not have sufficient pressure to achieve a good bond thus the crack resulted from the inability of the compact to hold the release wave. Figure 9b shows a magnified view of the fracture (non-consolidated) region. Evident here is the lack of any clear sign of interparticle melting. Note the circle which shows the original dendritic particle microstructure at the center of the polyhedral face. The gold coating appears to be highly cold worked and is evident at the powder particle interfaces, indicated with arrows.

Figure 10 illustrates the low pressure response of the two different density powders. The primary difference as shown by the arrows is in the radius of the melt zone interface. Since the pre-shocked diameters were equal, the higher density powder has a larger diameter. Note that in this pressure regime all the particles are nominally polyhedra right up to the melt zone.

The increase in temperature in the low density powder (Fig. 10a) has resulted in a superior compaction in the non-melted zone. The central radial cracks are confined to the melt zone. For the higher density material (Fig. 10b) the temperature is lower for comparable

radial cracks are interparticle and similar to those shown in Fig. 9. At higher pressure the lower initial density (Fig. 11a) has again a much larger melt zone illustrating the effect of higher entropic and strain heat [3]. The crack and macro voids are confined to the melt zone. The size of the solidification void (i.e., center hole) is not pertinent [10].

Similarly for the higher packing density powder the melt zone is smaller as it was at lower pressure. Inspite of the fact that the pressure for the 57% density was higher than for the 47% density. In this situation the particle strain is the more significant contributor to the residual temperature, consequently a smaller melt zone. While the outer diameter of the compacted powder in Fig. 11b has similar pressure as that of Fig. 10b, the bottom region has had approximately 12% local longitudinal strain normal to the micrograph. Note the compacted diameter is slightly smaller than the top (ie Fig. 11b vs Fig. 10b).

Figure 12 illustrates the pressure to melt versus initial powder density for the 304L SS. This curve divides the region between compaction/consolidation on the left and melting of the powder on the right and represents the upper limit of pressure to achieve consolidation for a given starting density. We were not able to establish the lower limit between good compaction and consolidation. The elimination of the melt zone can be achieved by simply incorporating a solid rod down the central axis of the holder as has been done by a number of experimenters. This minimizes the entropic and strain heat in the central axis which is the major heat contributor to the residual temperature.

V. DISCUSSION

On comparing the initial packing density with the shock response, it is evident that an increase in packing density decreases the melt region. This is obviously more desirable from a compaction point of view Although the experiments reported here did not attempt to compact near 90% theoretical density material, it would be, perhaps, the choice for

initial packing. Solid 304L SS shocked in the same design does not melt [3]. The reasons are the associated particle strain and concomitant temperature. As more and more of the interstitials are filled with smaller powder particles the local strain is reduced. This in turn reduces the temperature rise due to the strain heating discussed by [3]. In essence for good consolidation of 304L SS one needs to minimize (not eliminate) the temperature effect.

VI. CONCLUSIONS

The observations deduced from these experiments can be summed up as the following:

1. An increase in pressure, increases the entropic heat. For powders the entropic heat must include the collapse of the porosity.
2. An increase in local strain, increases the strain heat.
3. An increase in packing density decreases the strain heat but increases the entropic heat.
4. Even if the packing density remains the same (i.e., different monosizes) the number of contact points changes thus a change is strain heat.
5. Increasing the particle surface area increases the strain heat.
6. Mach stem melting occurs after apparent shock up to "full" density.
7. Green or packing density is shown to be a significant parameter in powder shock response.

VII. ACKNOWLEDGEMENT

The authors wish to thank the Los Alamos National Laboratory, Center for Materials Science for some financial support.

VIII. REFERENCES

1. R. Prummer, Vortrag, 4, 10 (1972).
2. R. B. Schwarz, et. al., Shock Waves in Condensed Matter, J. R. Assay, F. A. Graham, G. K. Straub, ed. Elsevier Sci. Pub. 435, (1983).
3. K. A. Johnson, K. P. Staudhammer, this proceedings.
4. K. A. Johnson, L. E. Murr, and K. P. Staudhammer, Acta. Metall. V33, 77 (1985).
5. H. D. Lewis, A Goldman, J. Am. Ceram. Soc. Vol. 49, 323 (1966).
6. A. E. R. Westman, H. R. Hugill, Am. Ceram. Soc., V13, 767 (1930).
7. D. R. Hudson, J. Appl. Phys. 20, 154, (1949).
8. W. M. Visscher, M. Bolsterli, Los Alamos National Laboratory Report LA-DC-72-745 (1972).
9. R. K. McGeary, J. of the American Ceramic Society, V44, 513 (1961).
10. K. P. Staudhammer and K. A. Johnson, APS Fourth Topical Conf. Shock Waves in Condensed Matter - 1985, Gupta. ed.

CAPTIONS

FIG. 1 Typical non-spherical 304L stainless steel powder.

FIG. 2 Typical as received spherical 304L SS powder.

FIG. 3 Pressure vs distance near the OD of the 57% theoretical density 304L SS powder (radial distance = 2.25 mm).

FIG. 4 Schematic of post shocked powder holder.

FIG. 5 Optical photomicrograph of melt and consolidated zones in 100 mesh 304L SS powder, cross section taken 3.8 cm from top. a) radial cross section b) higher magnification of melt zone c) interface of melt and consolidated zones.

FIG. 6 Optical micrograph of 170/325 mesh 304L SS gold coated powder, cross section taken at 5.1 cm from the top. Arrow indicates melt zone radius.

FIG. 7 Transition zone in 170/325 mesh gold plated 304L SS powder, cross section at 5.1 cm from the top. a) shock wave front orientation relative to consolidated morphology, b) Interface structure illustrates transparticle massive melting.

FIG. 8 Low pressure (0.70 Mbars) compacted region at 1.9 cm containing 170/325 mesh gold plated 304L SS powder.

FIG. 9 SEM of fracture in Fig. 8 a) illustrating polyhedral morphology, A is powder holder, b) showing the residual gold plating at arrows.

FIG. 10 Comparison of melt zones in 304L SS a) 100 mesh, initial packing density 47% to, b) 175/325 mesh, initial packing density 57% comparative pressures of $\sim$ 0.07 and $\sim$ 0.09 Mbar respectively.

FIG. 11 Comparison of melt zones in 304L SS a) 100 mesh, initial packing density 47% to b) 170/325 mesh, initial packing density 57%. Comparative pressures of $\sim$ 0.66 and $\sim$ 0.80 Mbar respectively.

FIG. 12 Packing density vs calculated pressure to melt.

F 1

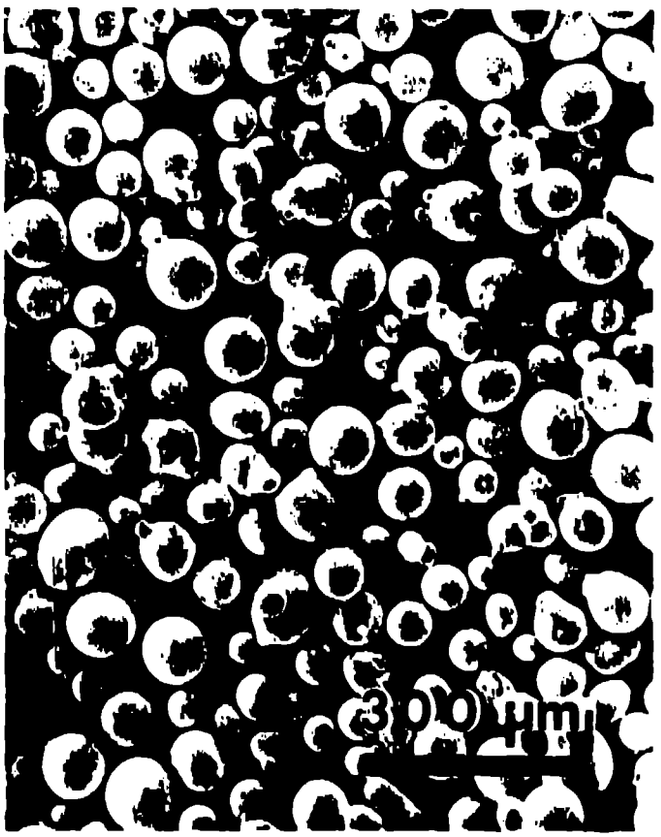

F 2

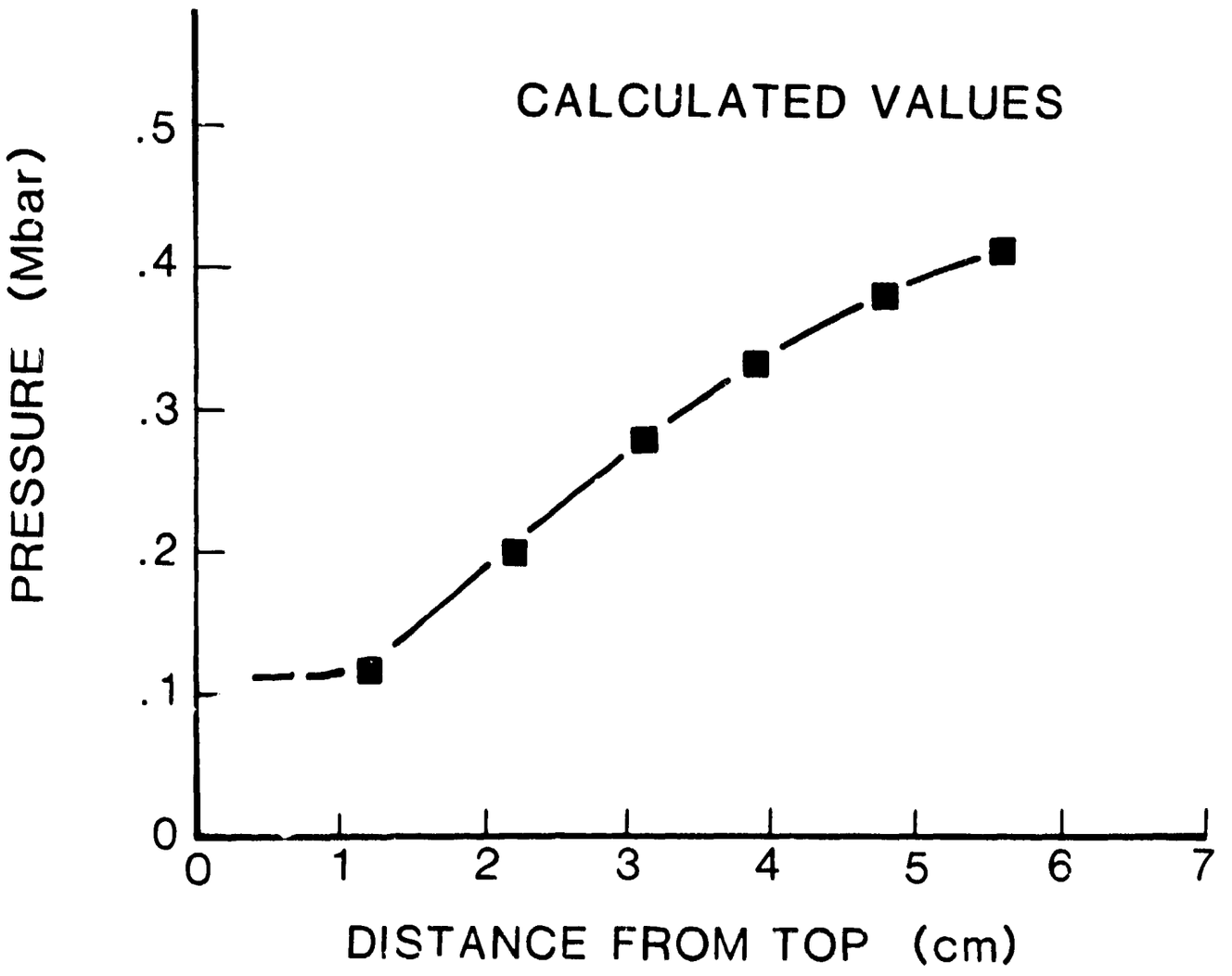
CALCULATED VALUES
PRESSURE (Mbar)
.5
.4
.3
.2
.1
0
0
1
2
3
4
5
6
7
DISTANCE FROM TOP (cm)

F3

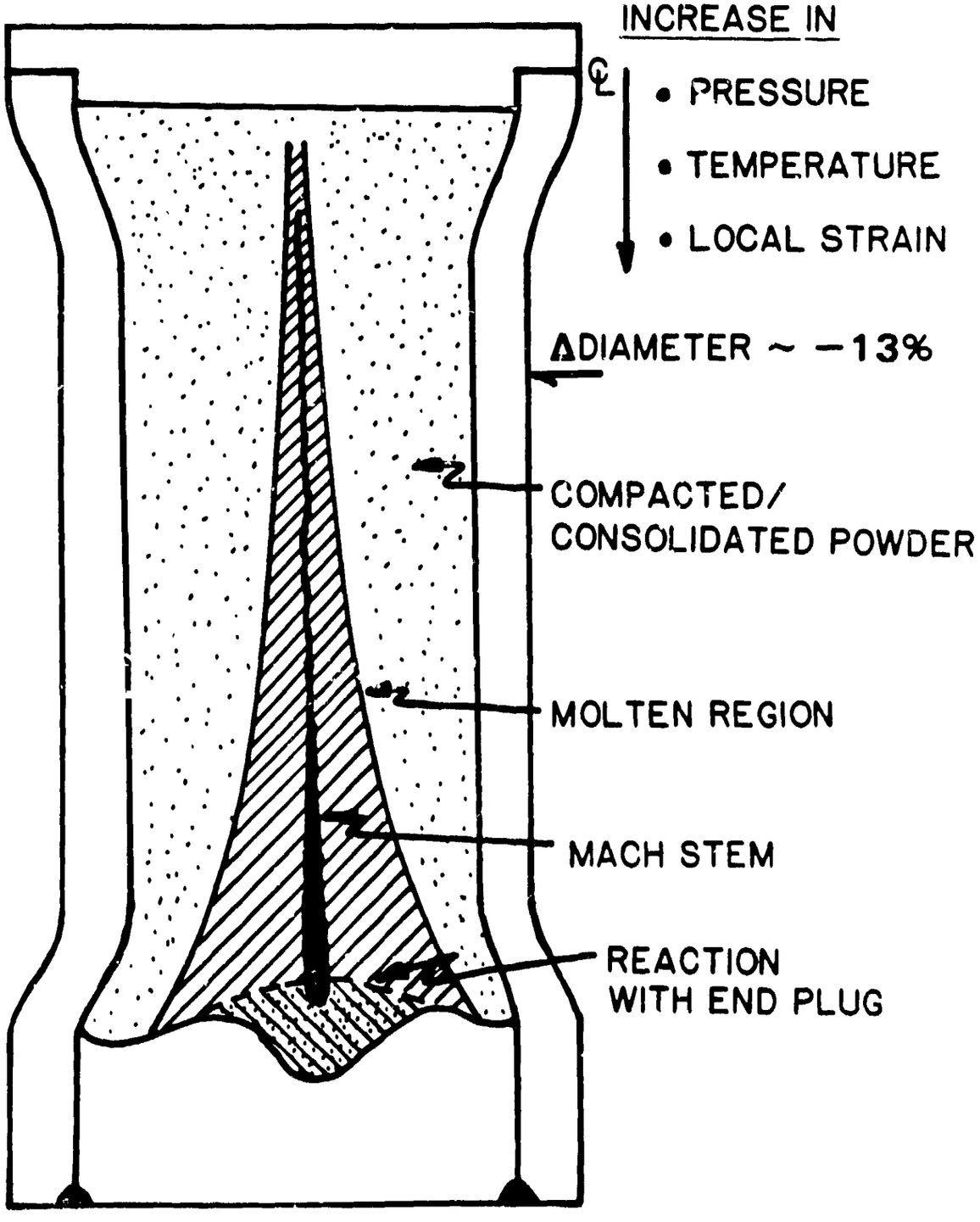
INCREASE IN
℄
• PRESSURE
• TEMPERATURE
• LOCAL STRAIN
ΔDIAMETER ~ −13%
COMPACTED/
CONSOLIDATED POWDER
MOLTEN REGION
MACH STEM
REACTION
WITH END PLUG

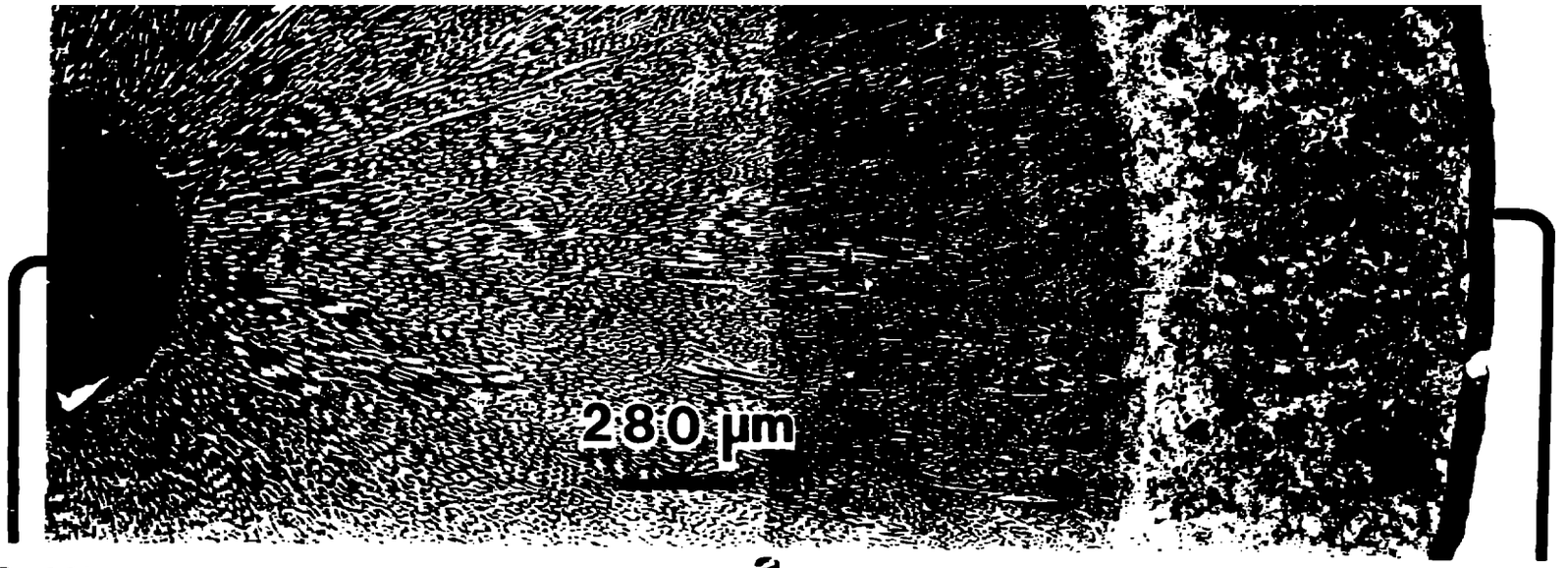

~.66 Mbar

a

~ .07 Mbar

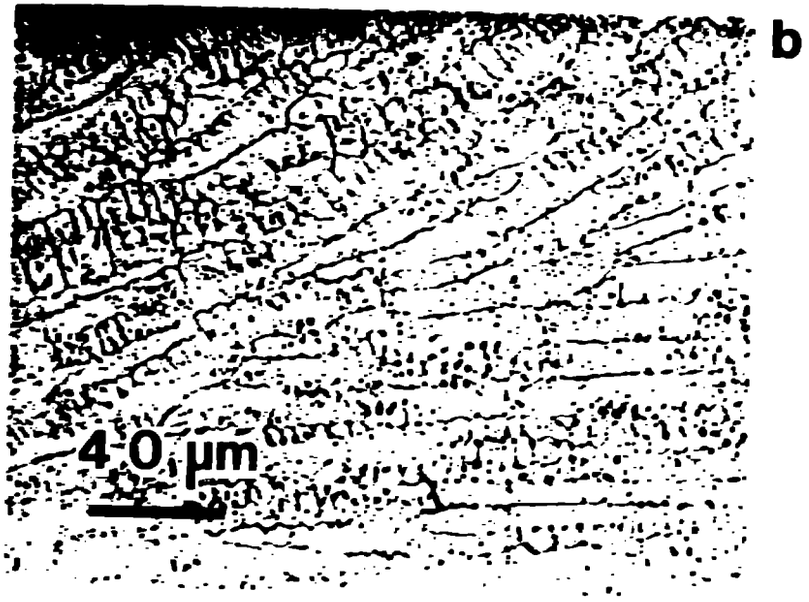

b

c

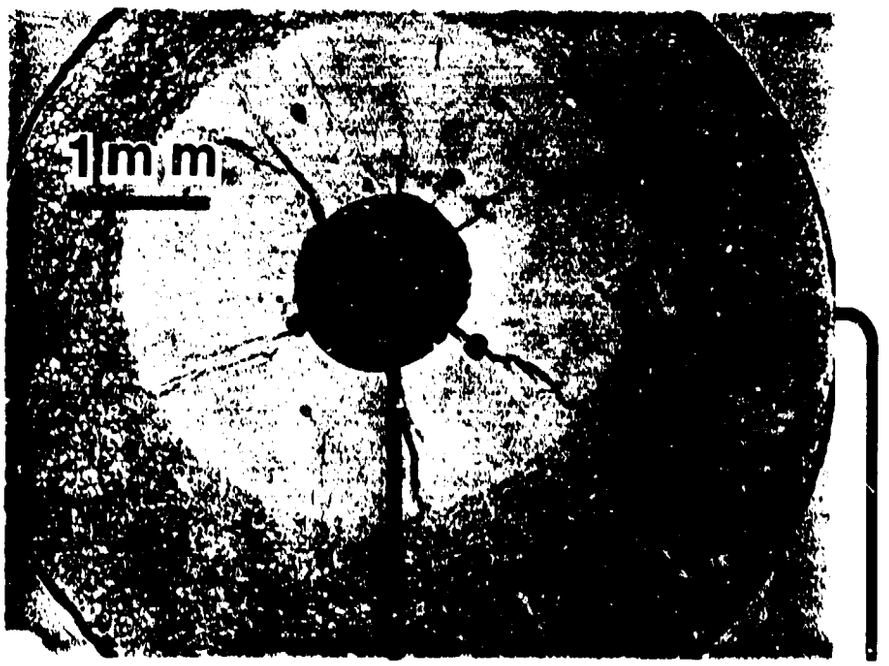
1 mm
~1.0 Mbar
~0.4 Mbar

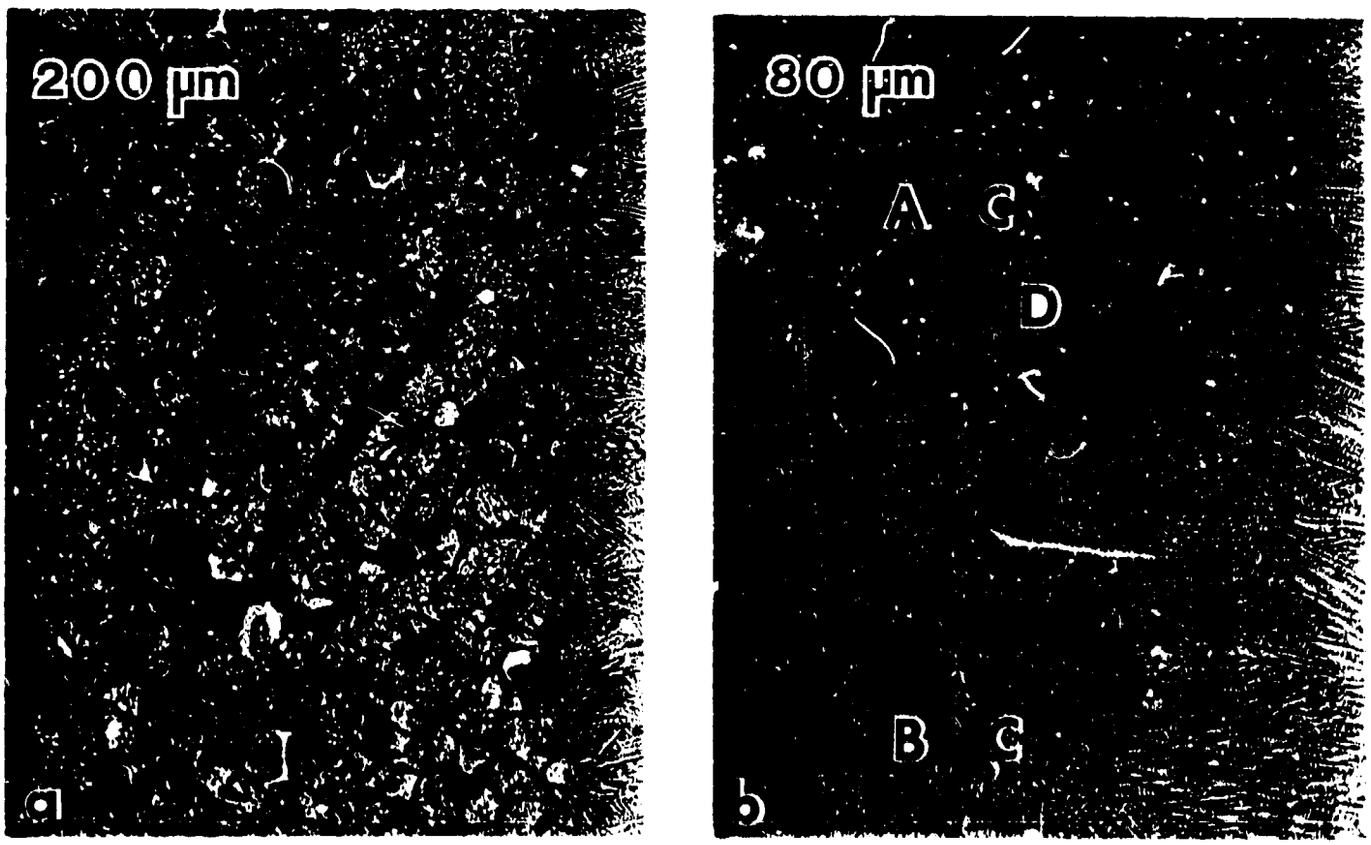
200 µm
a
80 µm
A
C
D
B
C
b


200 µm

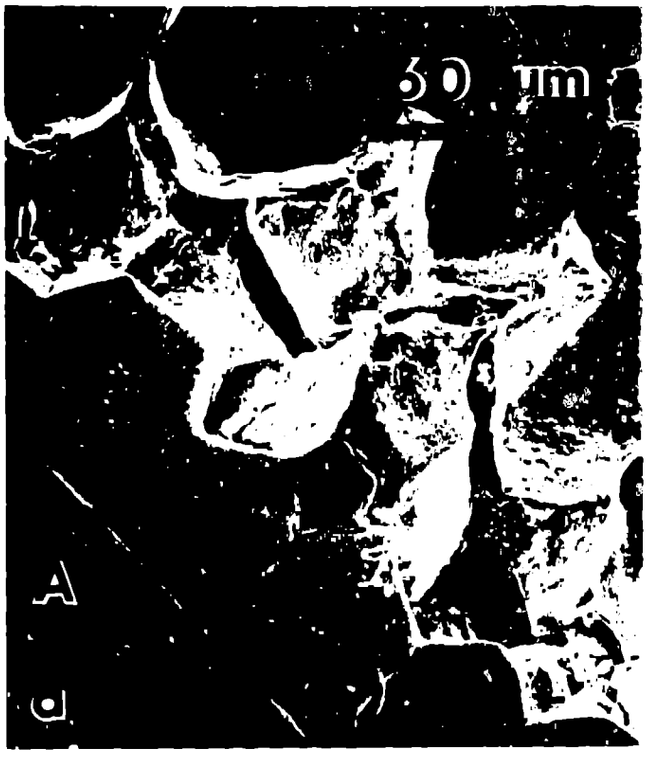
30 µm
A
a


30 µm
b

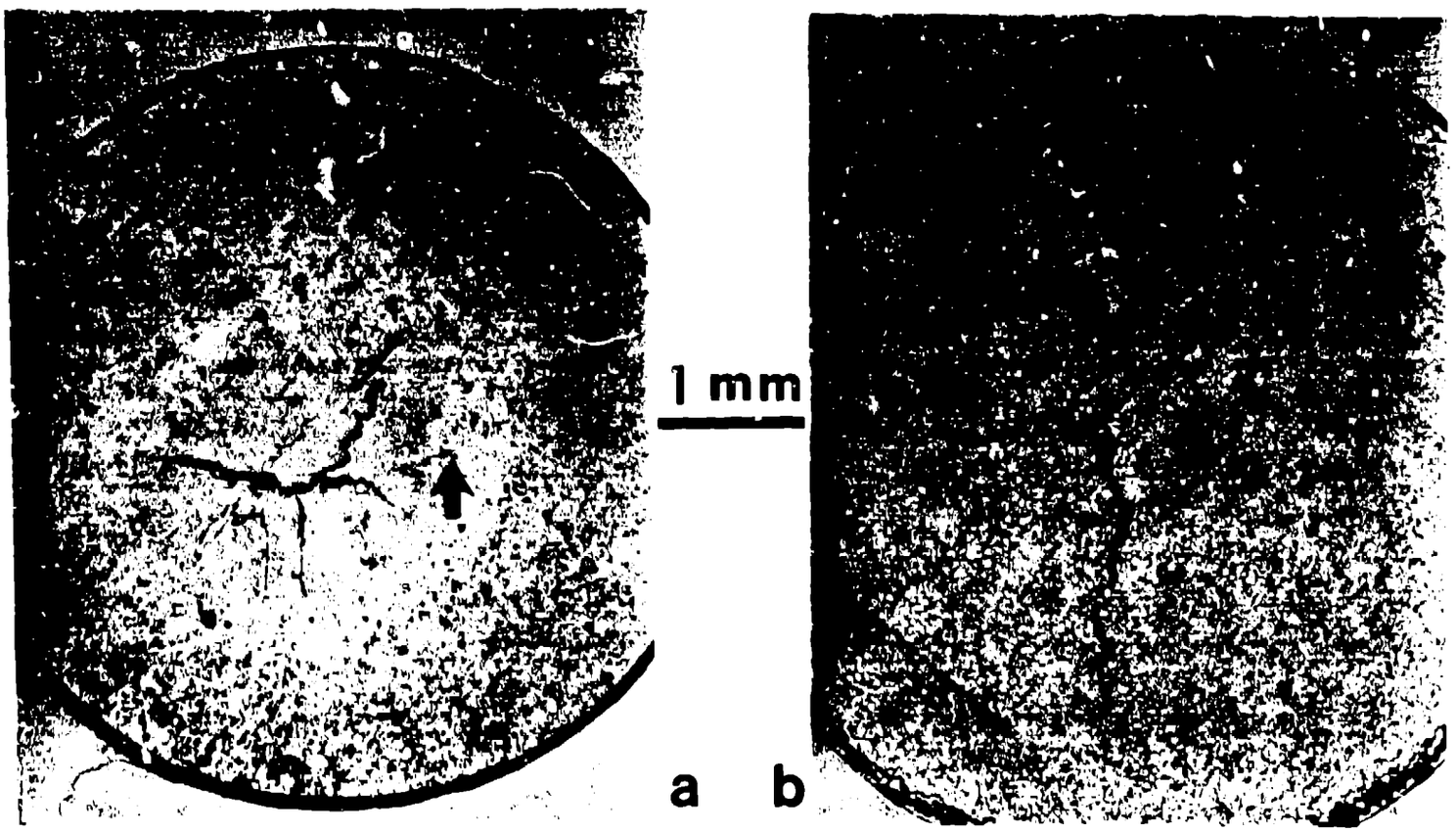
1 mm
a
b

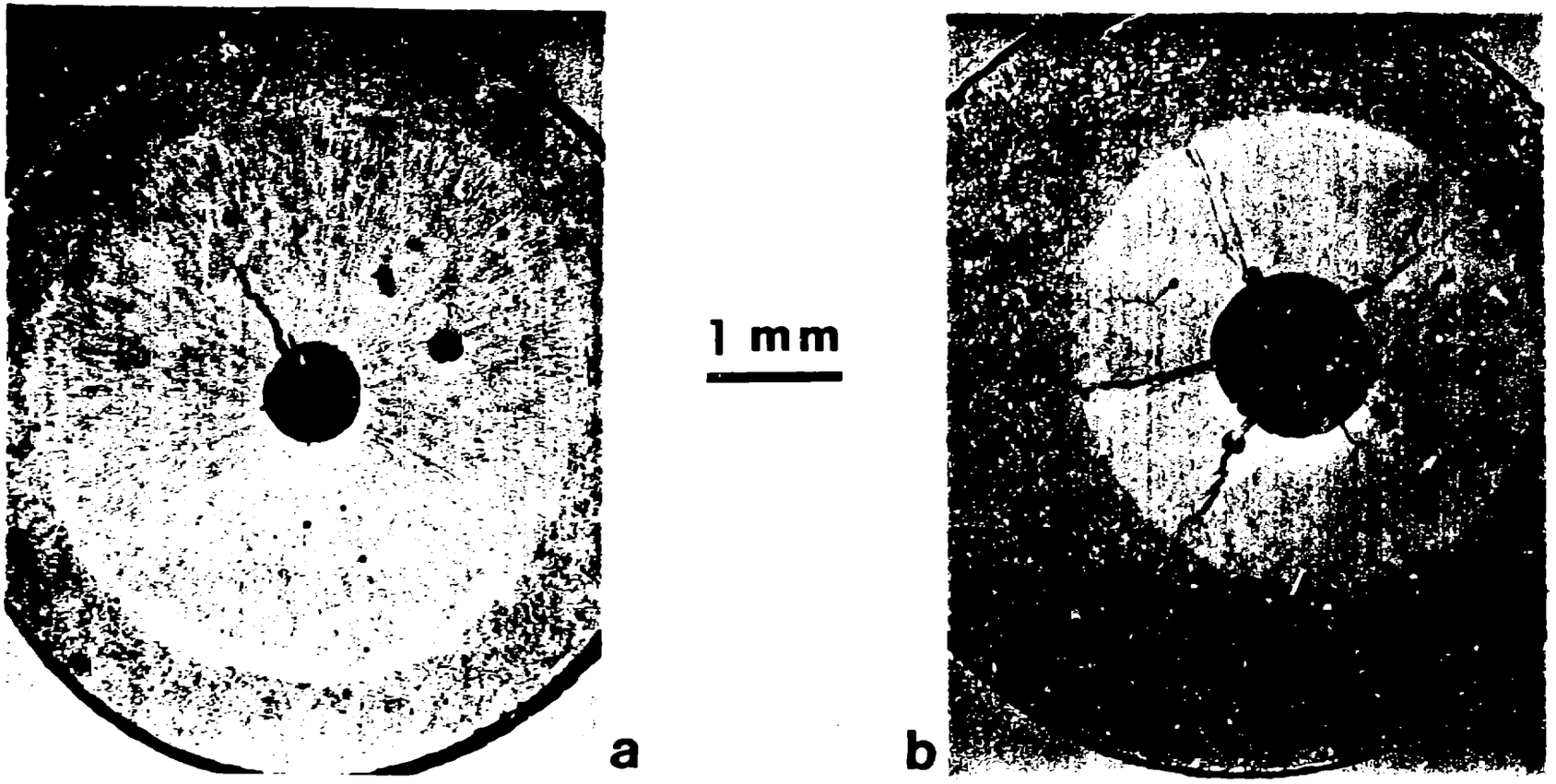
1 mm
a
b

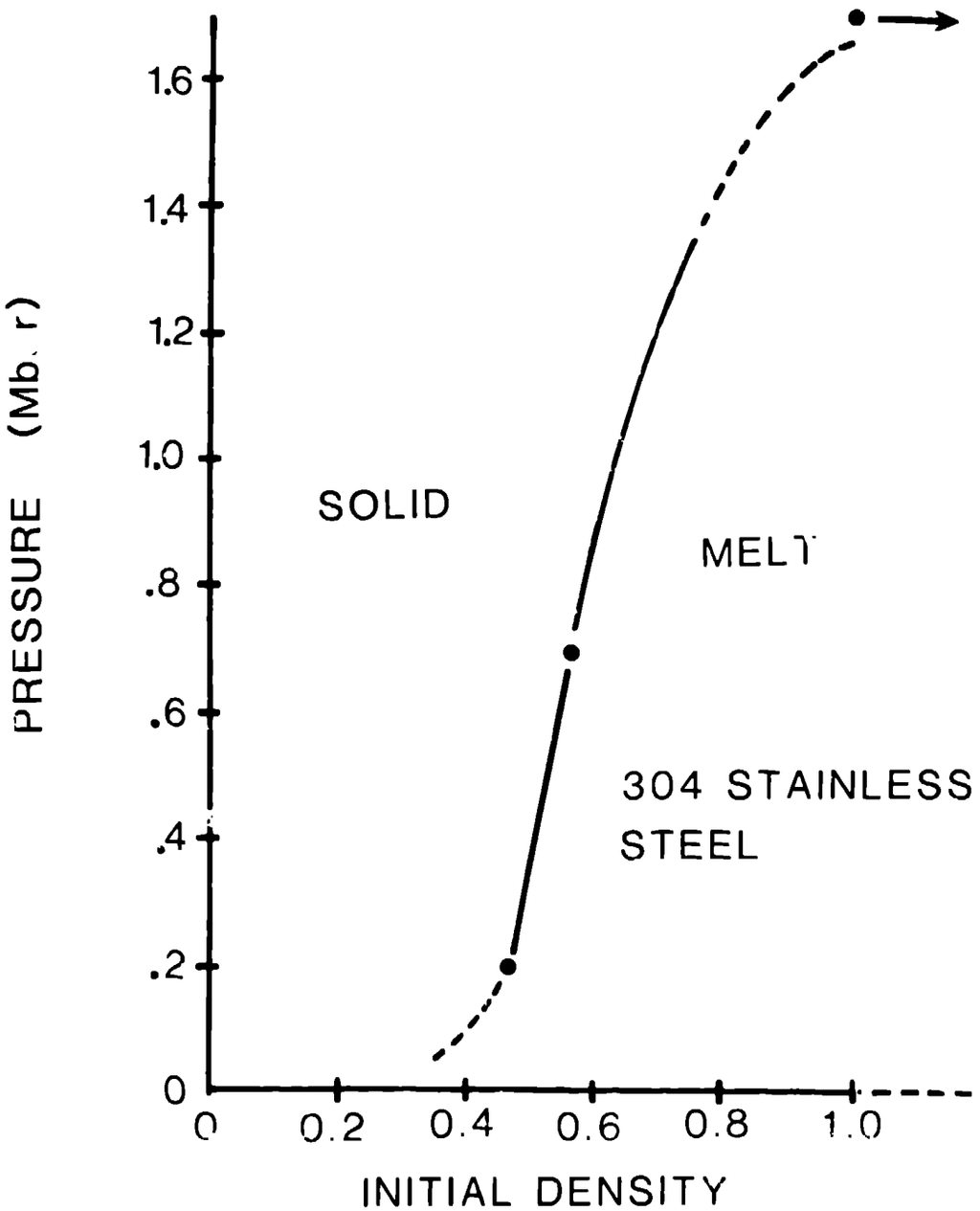
PRESSURE (Mb, r)
1.6
1.4
1.2
1.0
.8
.6
.4
.2
0
SOLID
MELT
304 STAINLESS
STEEL
0
0.2
0.4
0.6
0.8
1.0
INITIAL DENSITY

F12